






## Open Archive Toulouse Archive Ouverte (OATAO)

OATAO is an open access repository that collects the work of Toulouse researchers and makes it freely available over the web where possible

This is an author's version published in: <http://oatao.univ-toulouse.fr/24514>

**Official URL:** <https://doi.org/10.1016/j.addma.2018.02.005>

### To cite this version:

Ferrage, Loïc  and Bertrand, Ghislaine  and Lenormand, Pascal  *Dense yttria-stabilized zirconia obtained by direct selective laser sintering.* (2018) Additive Manufacturing, 21. 472-478. ISSN 2214-8604

Any correspondence concerning this service should be sent to the repository administrator: [tech-oatao@listes-diff.inp-toulouse.fr](mailto:tech-oatao@listes-diff.inp-toulouse.fr)

# Dense yttria-stabilized zirconia obtained by direct selective laser sintering

Loïc Ferrage<sup>a,\*</sup>, Ghislaine Bertrand<sup>b</sup>, Pascal Lenormand<sup>a</sup>

<sup>a</sup> CIRIMAT, Université De Toulouse, CNRS, INPT, UPS, Université Toulouse 3 Paul Sabatier, Bât. CIRIMAT, 118 Route de Narbonne, 31062 Toulouse Cedex 9, France

<sup>b</sup> CIRIMAT, Université De Toulouse, CNRS, INPT, UPS, ENSIACET, 4 Allée Emile Monso, CS 44362, 31030 Toulouse Cedex 4, France

## ARTICLE INFO

### Keywords:

Selective laser sintering

Additive manufacturing

Ceramic materials

Yttria-stabilized zirconia

## ABSTRACT

This work demonstrated the possibility to manufacture dense yttria-stabilized zirconia (YSZ) parts by direct laser beam sintering using a commercial 3D SYSTEMS machine. To achieve this, several requirements of the process itself had to be met. First, an efficient laser-matter interaction had to be achieved. Indeed, a major issue to overcome was the intrinsic nonabsorbance property of the YSZ powder at the Nd:YAG laser wavelength. This issue was solved by adding a small amount of graphite to the YSZ powder that resulted in a simple mechanical blending of the two compounds. The graphite adjunction allowed an increase in the absorbance value from 2% to approximately 60%. The chemical composition of the powder blend and the density and the particle size distribution of the starting material used in this work enabled adequate heat transfers due to the appropriate thermophysical properties. Finally, a set of machine parameters that allows to manufacture parts with a high relative density, good geometrical accuracy, and mechanical strength was experimentally determined. Ultimately, it was found that the direct SLS allows the reproducible manufacture of simple YSZ parts with a relative density of 96.5%.

## 1. Introduction

Selective laser sintering (SLS) is an additive manufacturing process that uses a laser beam as a power source to selectively sinter or melt a powder bed. Although this process is presently considered as a well suited technique for the production of metallic and polymer parts [1–4], the direct manufacture of ceramics by SLS remains challenging [5]. Indeed, most of the commercially available SLS machines are equipped with Nd:YAG laser (also called the fiber laser, with a wavelength of  $\lambda = 1.065 \mu\text{m}$ ). This near infrared wavelength is less absorbed by oxide ceramic powders [6], thereby resulting in a non-efficient laser material interaction and thus an unsatisfactory shaping.

The adaptation of the SLS process to the sintering of a new material is particularly complex. Indeed, the different physical properties (such as radiation absorbance, emissivity, or heat capacity) of different compounds have an impact on the amount of energy transferred to the powder under laser irradiation for similar processing conditions [7]. With regard to ceramic materials, if enough energy is not transferred to the powder, sintering does not occur. If this amount of energy is too high, particles are completely melted. In this case, the resulting “melting pool” rearranges to minimize its surface energy this phenomenon is even more accentuated for materials with a high melting point. Solidified droplets appear, thus leading to a nonconsolidated object. To address this issue, high melting point materials are often

blended with another compound that has a lower melting point a polymer binder for instance [8–11]. In this case, this process is referred to as indirect SLS. Absorption additives also can enhance the interaction between the laser beam and the powder. Ho et al. were the first to demonstrate that the addition of a small amount of graphite powder (up to 2% in weight) to a polycarbonate powder allowed the powder bed surface to reach a higher temperature under laser irradiation [7]. This observation was attributed to an increase in the absorption of laser energy. E. Juste et al. investigated the effect of graphite adjunction on the SLS of a ceramic [12]. They spray dried an alumina slurry previously mixed with a graphite based colloidal suspension. The resulting powder allowed the manufacture of complex shaped parts with relative densities of up to 90%.

The objective of the work is the additive manufacturing of yttria stabilized zirconia (YSZ) parts by direct SLS. In direct SLS, the parts are manufactured in a single operation where the geometrical shape and the material properties of the desired part are achieved simultaneously [13]. The advantage of the direct additive manufacturing is that it does not require a time consuming postprocessing step (no binder removal and subsequent sintering). The development of a new process to manufacture YSZ objects is particularly interesting, given its challenging intrinsic properties such as a low thermal shock resistance and a high melting temperature (2700 °C for zirconia stabilized by 8 mol% of yttria) and widespread applications. Zirconia is an electric insulator as a

\* Corresponding author.

E-mail address: ferrage@chimie.ups-tlse.fr (L. Ferrage).

pure compound but becomes an ionic conductor when doped, and the stable cubic  $ZrO_2 \cdot 8Y_2O_3$  structure is often used in fuel cells or oxygen sensors [14]. The good performances at higher temperatures make YSZ an appropriate material for thermal barrier, and it is used in the transportation industry as a protector of nickel superalloys to extend their use to temperatures above 1100 °C [15]. The chemical inertia, high flexural strength, and fracture toughness confer to this ceramic the required properties to be used as an implantable material for biomedical applications [16]. Previous work was done on the SLS of YSZ, but some limitations were observed. Bertrand et al. successfully manufactured low density parts (56%) [17], and Liu et al. were able to sinter denser parts (90%) by modifying the original process: the YSZ powder bed was subjected to high temperature preheating [18].

In the present work, tests were carried out using a commercial SLS machine to manufacture simple geometry parts of dense YSZ. Different operating parameter combinations were investigated with the aim of finding reproducible process conditions for shaping ceramics. The low absorbance of the powder in the far infrared region, which prevents an efficient energy transfer between the laser beam and the powder bed, was increased by mixing small amounts of graphite with the starting material. Effective operating parameters were determined, and some structural properties of the manufactured parts were investigated.

## 2. Powder characteristics

### 2.1. Starting materials

Yttria fully stabilized zirconia ( $ZrO_2 \cdot 8Y_2O_3$ ) provided by Tosoh was used in the present work. The shape of the powder particles is spherical (Fig. 1(a)), as generally recommended in SLS for an easy spread.

The size distribution is shown in Fig. 2, measured using Malvern Mastersizer 3000 by laser light scattering on dry powder. It reveals a large multimodal distribution with  $d_{10}$  of 3  $\mu m$ ,  $d_{50}$  of 14  $\mu m$ , and  $d_{90}$  of 50  $\mu m$ . These results are in accordance with the SEM observations.

Before conducting any work within the SLS machine and to ensure that this powder might be used for the SLS process, its flowability was evaluated by the measurement of its Hausner ratio ( $HR$ ) (Eq (1)). A powder with a good flowability is required for this process to ensure that the dedicated device will be able to correctly spread successive layers.  $HR$  is defined as the ratio of the tapped density  $\rho_T$  to the bulk density  $\rho_B$  of the powder in a container (see standard ASTM B527 [19]).

$$HR = \rho_T / \rho_B \quad (1)$$

A  $HR$  less than 1.25 is an indicator of good flowability. If  $HR$  is between 1.25 and 1.4, the flowability of the powder is poor, and if  $HR$  is greater than 1.4, the powder is cohesive. It was found that for the YSZ powder used in this study,  $\rho_T = 1.43 \text{ g cm}^{-3}$  and  $\rho_B = 1.22 \text{ g cm}^{-3}$ ; hence,  $HR = 1.17$ , which means that the powder can be easily spread.

The graphite powder used to improve the absorbance of YSZ has irregularly shaped particles with a  $d_{50}$  of 19  $\mu m$ , specific surface area of 9  $m^2/g$ , and density of 0.19  $g/cm^3$  (Fig. 1(b)).

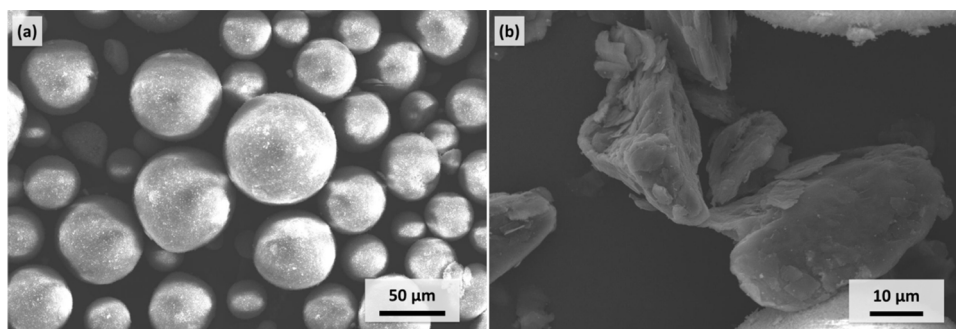


Fig. 1. SEM images of the yttria-stabilized zirconia powder used in the study (a) and the graphite particle used as an absorbing additive (b).

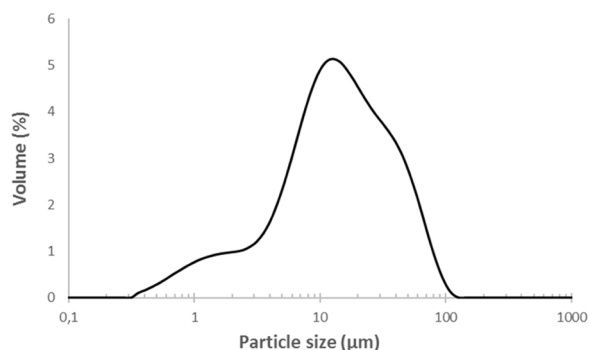


Fig. 2. Particle size distribution of the TZ-8Y powder, as provided by Tosoh.

### 2.2. Optical properties of the powders

Among other thermophysical and optical properties (such as thermal diffusivity and emissivity), absorbance at the laser wavelength is considered as one of the most important powder properties in SLS. Indeed, it is an intrinsic property that is observed regardless of whether a laser matter interaction can occur.

For this, the absorbance value  $A$  of the powder was investigated by spectrophotometry (AGILENT Spectrophotometer Cary 5000 UV vis NIR). The spectrophotometer enables the direct measurement of the reflectance  $R$ . The absorbance was then calculated according to Eq. (2):

$$A = I - R - T \quad (2)$$

where  $T$  represents the transmittance. For these measurements, powder samples were manually compacted and were approximately 3 mm thick. Thus,  $T$  was considered equal to zero.

It was found that the YSZ powder, as received from the manufacturer, exhibits an absorbance value of less than 2% at a wavelength  $\lambda$  of 1.065  $\mu m$ . Therefore, almost no energy is transferred to the powder when it is irradiated with a laser beam of this wavelength, and the resulting increase in temperature is not sufficient. To overcome this major issue, graphite with an absorbance value of 81% was added to YSZ to increase the absorbance of the powder. Small amounts of graphite were directly mixed with the YSZ powder.

Five blends with different YSZ graphite ratios (see Table 1) were prepared to analyze the optical properties, before choosing the optimum composition for sintering experiments.

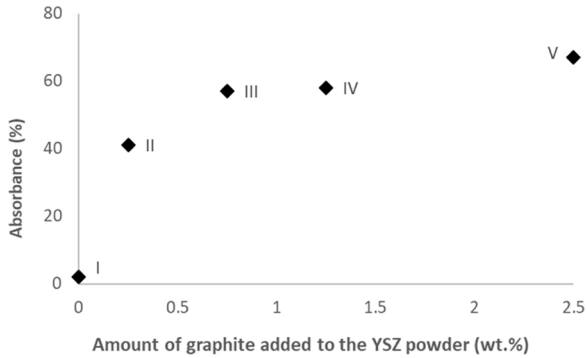
The two compounds were mechanically blended in a three dimensional Turbula shaker mixer for 1 h. A change in color was observed: the YSZ powder was white and the blends were light grey (the color became darker with the increase in the amount of graphite). The blended powders were sieved to 120  $\mu m$  to eliminate potential agglomerates or oversized particles. The absorbance of each blend was evaluated by spectrophotometry. The results showed that the absorbance increased to 67% for blend V with 2.5 wt.% of graphite, as shown in Fig. 3.

The absorbance measurements proved that the addition of an

**Table 1**

Composition of YSZ-graphite blends prepared for optical property analysis.

Blend	I	II	III	IV	V
Mass percent of graphite	0	0.25	0.75	1.25	2.5

**Fig. 3.** Evolution of the absorbance for different amounts of graphite in the powder mixture, at a wavelength of 1.065  $\mu\text{m}$ .

absorbing agent to the commercial powder changes the behavior of the powder for an incident beam at 1.065  $\mu\text{m}$ . Indeed, the YSZ graphite blend is capable of interacting with a Nd:YAG laser beam, thus undergoing thermal exchanges, even with small amounts of graphite, while YSZ powder as a single material reflects almost all the energy delivered by the laser beam. This result is particularly interesting because unlike similar work that has been done previously on alumina [12], here the YSZ graphite blend is a simple physical mixture that does not require any chemical treatment or new powder production and is, thus, easily and quickly prepared.

For the following experiments, we chose powder blend III with 0.75 wt.% of graphite (4.6 vol.%), which corresponds to an absorbance value of 57% sufficiently close to the that of metallic powders that are traditionally used in the selective laser melting process (for comparison purposes, the absorbance of aluminum alloy AlSi12, stainless steel 316L, and titanium alloy TA6 V were measured: 62%, 69%, and 64%, respectively).

As this amount of graphite is small (0.75 wt.%, which corresponds to 4.6 vol.%), it does not impact the Hausner ratio and therefore the flowability of the powder.

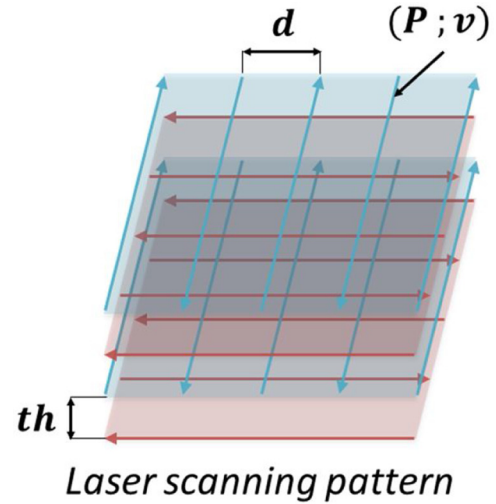
### 3. Selective laser processing

#### 3.1. SLS equipment

For this study, a commercial SLS machine, ProX200 from 3D Systems, was used. The machine is equipped with Nd:YAG laser emitting at a wavelength of 1.065  $\mu\text{m}$ , with a maximum power of 300 W. The building platform dimensions are  $140 \times 140 \text{ mm}^2$ , and the parts can reach a maximal height of 100 mm. All process parameters can be modified by the user, regardless of whether they are laser parameters (e.g., scan speed, power) or layer spreading parameters (e.g., layer thickness, compaction rate). For the experiments, the building chamber was maintained at room atmosphere. After each experiment, the loose powder was collected and sieved so that it can be re used for subsequent trials.

#### 3.2. Sintering experiments

Once the optimum blend composition was determined, the focus of the experimental work was on the SLS machine parameters. Adjusting all parameters allows to control both the powder spreading and the laser irradiation specifications. Therefore, for different combinations of

**Fig. 4.** SLS machine parameters.

the parameters, the volume of the irradiated powder and the amount of energy transferred to it are different. There are a large number of machine parameters; therefore, to limit the experimental work to a reasonable number of trials, we focused on five parameters that have an important impact on the laser matter interaction:

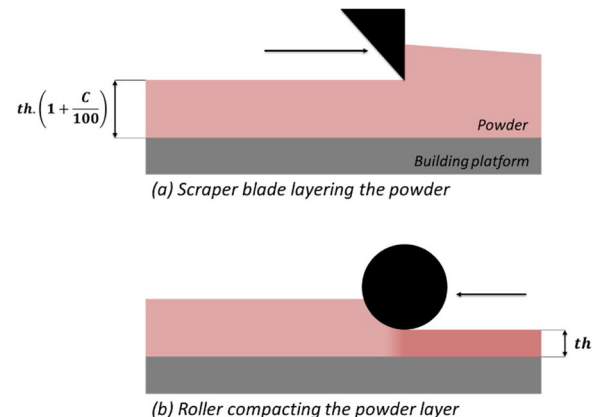
- Laser power  $P$  (W) (Fig. 4)
- Laser scan speed  $v$  (mm/s) (Fig. 4)
- Hatch distance  $d$  ( $\mu\text{m}$ ), defined as the distance between two consecutive laser tracks on the same layer (Fig. 4)
- Layer thickness  $th$  ( $\mu\text{m}$ ) (Fig. 4)
- Compaction rate  $C$  (%), defined as the thickness ratio added to the layer thickness before compaction (Fig. 5)

For experimental investigations, the upper and lower limits were set for each of these parameters (Table 2). The limits were either imposed by the SLS equipment and the powder characteristics or suggested by previous work reported in the literature [18,20,21].

For all the experiments, the same scanning strategy was used: each surface was scanned by parallel laser tracks. At every other layer, the direction of the laser tracks changed by  $90^\circ$  (Fig. 4).

#### 3.2.1. Powder layering on the building platform

The first step in the determination of optimum process parameters is the successful spreading of powder layers. For additive manufacturing processes, an optimum powder bed should be a continuous and homogeneous layer of powder easily spreadable on the building

**Fig. 5.** Powder layering (a) and compacting (b) steps.



**Table 2**

Processing windows for the parameters investigated.

Parameters	Laser parameters			Powder layering parameters	
	P (W)	v (mm/s)	d ( $\mu\text{m}$ )	th ( $\mu\text{m}$ )	C (%)
Ranges of values tested	30–100	10–1500	30–80	80–180	0–500

platform and on the top of another layer. The layers of powder should be as thin as possible to obtain an object with maximum resolution and surface finishing. The minimal thickness  $th$  and the compaction rate  $C$  were experimentally determined using the dedicated spreading device of the SLS machine. For the layering tests, at least 30 layers of powder were spread one above the other. The tests were considered successful if each layer of powder completely covered the building platform or the previous powder layer underneath and if each layer was visually observed to be homogeneous.

The powder dispenser of the additive manufacturing machine consists of a powder reservoir to provide a controlled volume of raw material. For every layer, a combined device of scraper blade and roller spreads the powder on the building platform, as such or compacted (see Fig. 5).

For the whole range of thicknesses tested with the YSZ powder, it was not possible to spread a continuous layer unless compaction was applied to the powder. The minimal compaction rate necessary for meeting the spreading of at least 30 successive layers was 300%. Similarly, for compaction rates of 300% and above, a thickness of at least 100  $\mu\text{m}$  was found to be necessary to obtain continuous and homogeneous layers. The given values are theoretical and correspond to the machine instructions. The actual layer thickness was evaluated by sliding a measurement comb, Elcometer 155, along the surface of a single compacted powder layer. The measurement teeth marks allowed obtaining a range of values including the real thickness, which was estimated to be between 100 and 125  $\mu\text{m}$ . This achieved value is finally in good agreement with the expected one.

### 3.2.2. Selective laser processing of the powder blend

The second step in the sintering experiments is the determination of optimum laser parameters. To achieve this, basic geometrical parts were produced. The laser power  $P$ , scan speed  $v$ , and hatch distance  $d$  were varied at a constant layer thickness of 100  $\mu\text{m}$  and compaction rate of 300%.

The SLS experiments were conducted according to the following procedure: first, a set of parameters is assigned to a part, using a specific software. The parts to be produced were square based cuboids with dimensions varying from  $5 \times 5 \times 3$  to  $18 \times 18 \times 6 \text{ mm}^3$ . For the smallest parts, up to 100 objects with different sets of parameters were produced on the same building platform, while for the bigger parts, 16 objects were produced. Then, the selective laser processing of the powder was performed, using blend III as the starting material. At the end of each experiment, the loose powder surrounding the parts was brushed away so that it can be recycled, and the building platform supporting the printed parts was removed from the SLS machine to observe the results.

For each experiment, the results were evaluated according to three criteria:

The presence of consolidated YSZ

**Table 3**

Laser power, scan speed, and hatch distance values tested in the first set of screening experiments.

Exp 1	Level 1	Level 2	Level 3	Level 4	Level 5	Level 6	Level 7	Level 8	Level 9	Level 10
P (w)	30	38	46	54	62	70	78	86	94	100
v (mm/s)	10	50	100	200	300	500	750	1000	1250	1500
d ( $\mu\text{m}$ )	30	50	80							

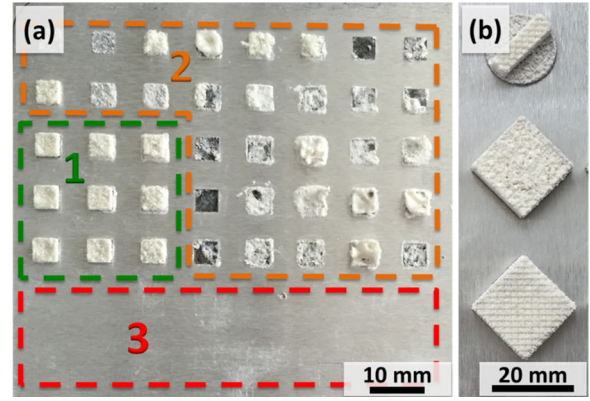


Fig. 6. Manufactured parts, as a result of the screening experiment (a) and obtained with the most satisfactory parameter combination (b).

The capacity of the consolidated part to be manipulated without crumbling

The accuracy of the geometry described in the CAD file.

To have a comprehensive overview of the combined influence of  $P$ ,  $v$ , and  $d$  on the laser sintering of YSZ powder, a screening methodology was used: several levels with different values for each parameter were tested, ranging across the entire window of values investigated. The sintering experiments were conducted using all possible combinations of levels of the three parameters. As an example, Table 3 details the levels tested in the first set of experiments.

The results showed that the window of values investigated was narrowed around the most satisfactory results; therefore, new levels of values were determined for the next set of experiments.

Fig. 6(a) illustrates the different possible outcomes resulting from 56 different sets of parameters assigned to 56 objects. In zone “1,” all three criteria were met. In zone “2,” the resulting parts could not be manipulated and/or the accuracy of the geometry was not satisfactory. In zone “3,” none of the criteria was met. Therefore, the upper and lower levels of  $P$ ,  $v$ , and  $d$  for the subsequent experiments were the same as those used to manufacture objects in zone “1.”

Satisfactory values were determined stepwise for every parameter, as detailed in Table 4.

Reproducibility of the SLS of the powder blend with this set of parameters (using  $P = 84 \text{ W}$  and  $v = 70 \text{ mm/s}$ ) was proven by manufacturing 40 samples used for further characterizations and by manufacturing objects with larger dimensions and different geometries (Fig. 6(b)).

## 4. Microstructural characterization of the manufactured parts

The above discussed approach was used to manufacture samples for structural and microstructural analysis. Several techniques were implemented to obtain a multiscale characterization of the ceramic objects produced by SLS.

Both the visual observation of the manufactured objects and optical microscopy observations of the cross sections (parallel to the building direction, Fig. 7(a)) indicate that the consolidated YSZ is dense and continuous (we cannot distinguish the successive layers of matter), except some cracks. This continuous nature of layers is consistent with

**Table 4**

Satisfactory ranges of values obtained after screening experiments.

Parameters	Laser parameters			Powder layering parameters	
	P (W)	v (mm/s)	d ( $\mu\text{m}$ )	th ( $\mu\text{m}$ )	C (%)
Satisfactory values	78–87	60–75	50	100	300

the fact that between consolidated layers, no delamination occurs during the fabrication or in the final objects. The objects can easily be manipulated with no damage and with an apparent isotropic strength. The surface of the objects was smooth and glassy, as shown in Fig. 7(b). The additively manufactured objects were white, contrasting with the gray powder, thus revealing an elimination of the graphite introduced in the starting material.

Scanning electron microscopy (JEOL JSM 6510LV) was performed on the fracture surfaces to characterize the surface parallel to the building direction.

Fig. 8(a) reveals an original microstructure composed of a succession of columns oriented along the building direction. Each column is subdivided into a stacks of grains with an elongated shape (shown in Fig. 8(b)) such that the longest dimension is perpendicular to the building direction. The microstructure of this ceramic is unusual and different from that of the same starting material (blend III) shaped with a conventional process (uniaxial pressing and sintering at 1600 °C for 2 h, Fig. 9). Therefore, the columnar microstructure is a result of the SLS of the YSZ graphite powder blend. The average width of the columns was measured as  $50 \pm 8 \mu\text{m}$  using the image processing software ImageJ. Similarly, it was found that the thickness of the lengthwise grains was  $10 \pm 2 \mu\text{m}$ . Even though the column width was in good accordance with the hatch distance used during the manufacturing of the observed object, the present work does not provide any evidence of a direct link between the hatch distance and the column dimensions. The microstructure characteristics might rather be a consequence of the combination of several parameters including the laser spot size. An experimental work remains to be conducted to determine how these parameters influence the ceramic microstructure.

Some pores with a mean size of  $1 \mu\text{m}$  or less were visible on SEM micrographs. The overall structure did not exhibit larger pores but had abundant cracks, mainly in between the columns. These observations were supported by macroscopic density measurements. The density of the YSZ starting material was measured using a helium pycnometer on the nonsintered dense powder particles. A mean value was calculated from the results of 10 measurements:  $d_{\text{YSZ}} = 5.985 \pm 0.002 \text{ g cm}^{-3}$ . The density of the bulk ceramic obtained by SLS in water was evaluated by the Archimedes method. A mean value was obtained from 3 measurements on 10 different samples. The density of the samples sintered with optimum parameters was  $d_{\text{part}} = 5.770 \pm 0.020 \text{ g cm}^{-3}$ . Thus, the relative density of the sintered YSZ parts was 96.5%. This relative density is higher than the one mentioned in the literature for the direct laser sintering of YSZ (up to 90%) [17,18] and even for indirect manufacturing (using a polymer binder, up to 92%) [8].

The crystallographic structure of the powders and the manufactured parts was investigated using an X ray diffractometer (BRUKER AXS D4 Endeavor, operating with a Cu K $\alpha$  radiation source of  $\lambda = 1.5418 \text{ \AA}$ ). X ray diffractograms of the raw powder and a laser sintered part (Fig. 10) showed that the crystalline structure of both materials is cubic (space group Fm 3m). No amorphous phase was detected, despite the “glassy nature” described previously. Blending of YSZ powder with graphite before the laser sintering step had no apparent impact on the nature of the phases present in the manufactured objects. Lattice parameters were calculated from the XRD data:  $a = 5.138 \pm 0.002 \text{ \AA}$  for the powder and  $a = 5.134 \pm 0.002 \text{ \AA}$  for the manufactured part, which is in accordance with the literature [22] and the JCPDS file no. 01 070 4436. These very close values are another indication that the crystalline structure and the chemical composition of the material did not change during the laser treatment.

The comparison of the two XRD patterns reveals a refinement of the peaks for the YSZ part sintered by SLS. Such a refinement indicates an increase in the crystallite size. This observation is supported by the calculation of the apparent crystallite mean size by the Scherrer method (Eq. (3)) as follows [23,24]:

$$L_{hkl} = 0.9 \lambda / (\beta \cdot \cos(\theta)) \quad (3)$$

where  $\lambda$  is the wavelength of the incident beam,  $\beta$  is the full width at half maximum, and  $2\theta$  is Bragg’s angle for the peak considered. The crystallite mean size was 36 and 118 nm for the raw powder and sintered parts, respectively. The crystallite growth was a consequence of matter transportation, which was activated thermally. This observation proves that despite the intrinsic low absorptivity of the YSZ powder that prevents a direct absorption of heat, the adjunction of graphite in the starting material allows thermal transfer to the ceramic. The particles of graphite absorb and transmit the heat before a plausible oxidation. By comparing the relative intensity of the peaks for both patterns, variations in the scattering intensity were observed. This was due to the preferred orientations, corresponding to the planes (220) and (311), in the YSZ parts manufactured by SLS.

## 5. Discussion

Shaping ceramic parts by consolidating successive powder layers in a SLS machine requires the conversion of the energy of a laser beam into thermal energy. The ceramic powder has to reach a temperature high enough to allow material diffusion and grain bonding, thus resulting in sintering. It is reported in the literature that this energy conversion is often a result of an optimization of the parameters listed in Section 3.2. However, regardless of these parameter values and considering the very low absorbance of YSZ powder at  $1.065 \mu\text{m}$  (pure YSZ powder absorbs less than 2% of the energy delivered by the laser beam), the resulting energy conversion does not allow to reach sintering or melting conditions.

A laser beam can interact with materials and induce modifications in different ways. For ceramics, lasers have been employed for machining pieces (by focusing the laser beam on the surface of the work

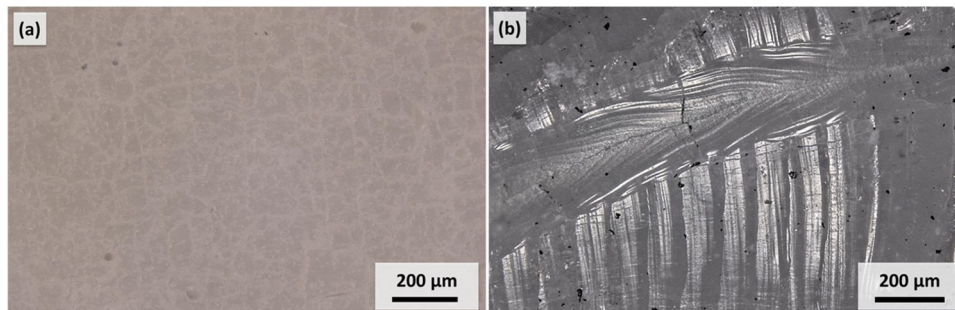


Fig. 7. Cross-section (a) and surface (b) pictures of an YSZ object prepared by SLS.

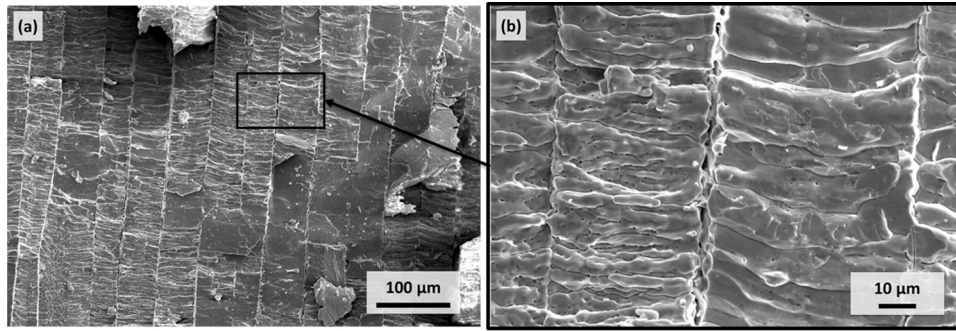


Fig. 8. SEM micrograph of a fracture surface of a laser-sintered YSZ part.

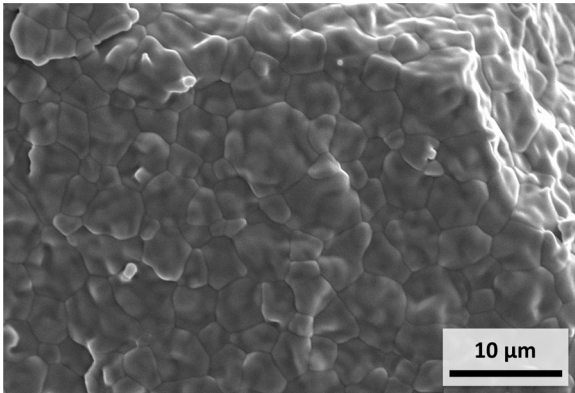


Fig. 9. SEM micrograph of a fracture surface of an YSZ part, manufactured by a conventional process.

part, the matter can melt, decompose, dissociate, evaporate, or be expelled) [25], or for densification purposes [26,27] with the aim to impact the microstructure and the properties of the treated material. The laser matter interaction depends on the thermophysical and optical properties of the irradiated material (density, emissivity, thermal conduction, specific heat, thermal diffusivity, and optical absorption), the dimensions of the sample, and the laser characteristics (energy and wavelength). When a laser beam impacts a material surface, two types of interactions are possible: a thermal interaction (the electromagnetic energy transported by the beam is converted into heat, which is partially or totally absorbed and driven in the material to a certain area and a certain depth, depending on its thermal conduction) or a photo ablation interaction (for short impulses, electrons are released, and some phase changes can be observed) [28]. For SLS, the objective is to achieve a thermal interaction between the laser beam and the surface of the powder bed.

Once a coupling of the ceramic powder and the laser at  $1.065 \mu\text{m}$  is achieved, all the conditions for a good energy conversion are not necessarily reached. Heat transfers within the powder should also be considered. In a powder bed, the heat transfers depend not only on the chemical composition of the particles and their thermal conduction but also on the powder density, particle size, and material volume weight (which impacts the contact thermal conductivity, radiative thermal conductivity, and volumetric specific heat, respectively) [29]. Therefore, in addition to the determination of optimum laser parameters, finding suitable powder layering conditions is also crucial. The increase in temperature should be induced at a depth deeper than a layer thickness to affect all the layers of the material in the irradiated area and to ensure the cohesion between layers.

Depending on the nature of the material treated and the temperature reached, different binding mechanisms may occur (solid state sintering, chemically induced binding, liquid phase sintering, full melting) [30]. In this work, we obtained consolidated ceramic objects from a powder. Although the binding mechanism is not yet clearly identified, it can be stated that a thermal interaction between the Nd:YAG laser and the YSZ powder bed was achieved. Restricted surface domains attained elevated temperatures in very short periods of time, making it difficult to determine whether the YSZ powder reached its melting temperature of approximately  $2700^\circ\text{C}$ . However, heat transfers occurred, meaning that the particle size and powder density were well adjusted and matched with the chemical composition, thermal conduction, and volume weight of the powder blend. While spectrophotometry measurements proved that a YSZ graphite blend is able to absorb the laser wavelength, SLS experiments highlight that this composite powder is suitable for the sintering process. A similar method that uses graphite as an absorbent agent for the additive manufacturing of alumina has already been reported in a previous work [12]. In the present work, the use of graphite allowed the manufacture of YSZ, which is a material with a high melting point ( $T_{\text{melt}}(\text{YSZ}) = 2700^\circ\text{C} > T_{\text{melt}}(\text{Al}_2\text{O}_3) = 2070^\circ\text{C}$ ), thus requiring more

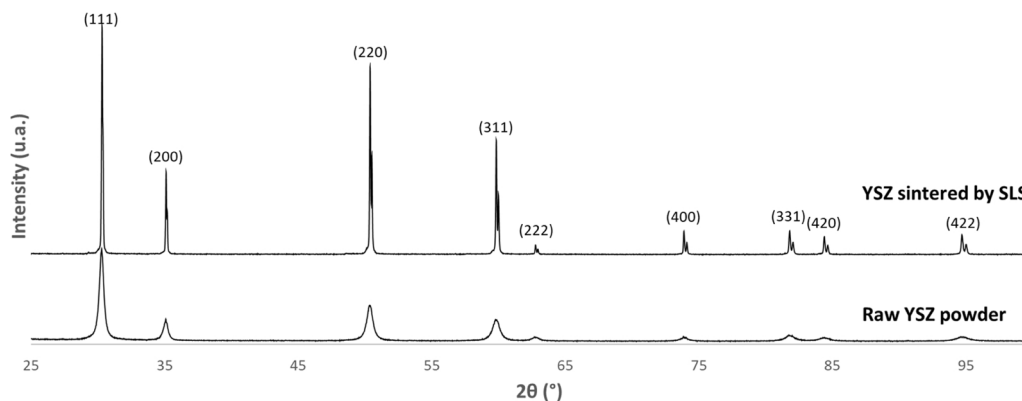


Fig. 10. XRD patterns of raw YSZ powder and laser-sintered YSZ part.



energy for shaping.

## 6. Conclusion

It is stated in the literature that oxides have a very low absorbance in the near infrared region (and in particular at 1.065  $\mu\text{m}$ , the wave length of the Nd:YAG laser). In this study, experiments showed that YSZ exhibits an absorbance value under 2%, which is not sufficient to perform the direct SLS of this material using a commercial machine equipped with a Nd:YAG laser.

It was found that the addition of a small amount of graphite (less than 5% vol.) to the YSZ powder increased the absorbance of the resulting blend by 50–60%. This improved absorbance allowed an efficient laser-matter interaction and heat transfers in the irradiated powder (resulting in a probable oxidation of the graphite and thus its elimination).

By using this powder blend composition and an optimum set of process parameters, it was possible to manufacture YSZ parts characterized by a high relative density of 96.5%.

However, consolidation mechanisms have not yet been properly explained. As the determination of the local temperature evolution during the irradiation of the powder surface might help to understand these mechanisms, studies remain to be conducted on this topic in the near future.

In addition, the microstructure of the parts obtained in the study is original and different from those of the YSZ parts sintered by traditional processes. This microstructure has a specific orientation, following the building direction. However, further studies are necessary to determine to what extent the laser scanning conditions can affect the microstructure of the resulting object.

## Acknowledgments

This research was supported by the ANR “Agence Nationale de la Recherche.” Loïc Ferrage would like to thank CIRIMAT Carnot Institute for the financial support of his PhD funding.

## References

- [1] W.E. Frazier, Metal additive manufacturing: a review, *J. Mater. Eng. Perform.* 23 (2014) 1917–1928, <http://dx.doi.org/10.1007/s11665-014-0958-z>.
- [2] J.W. Stansbury, M.J. Idacavage, 3D printing with polymers: challenges among expanding options and opportunities, *Dent. Mater.* 32 (2016) 54–64, <http://dx.doi.org/10.1016/j.dental.2015.09.018>.
- [3] I. Yadroitsev, P. Bertrand, I. Smurov, Parametric analysis of the selective laser melting process, *Appl. Surf. Sci.* 253 (2007) 8064–8069, <http://dx.doi.org/10.1016/j.apsusc.2007.02.088>.
- [4] S.F.S. Shirazi, S. Gharekhani, M. Mehrali, H. Yarmand, H.S.C. Metselaar, N.A. Kadri, N.A.A. Osman, A review on powder-based additive manufacturing for tissue engineering: selective laser sintering and inkjet 3D printing, *Sci. Technol. Adv. Mater.* 16 (2015) 033502, <http://dx.doi.org/10.1088/1468-6996/16/3/033502>.
- [5] L. Ferrage, G. Bertrand, P. Lenormand, D. Grossin, B. Ben-Nissan, A review of the additive manufacturing (3DP) of bioceramics: alumina, zirconia (PSZ) and hydroxyapatite, *J. Aust. Ceram. Soc.* 53 (2017) 11–20, <http://dx.doi.org/10.1007/s41779-016-0003-9>.
- [6] Nikolay K. Tolochko, Yurii V. Khlopov, Sergei E. Mozharov, Michail B. Ignatiev, Tahar Laoui, Victor I. Titov, Absorbance of powder materials suitable for laser sintering, *Rapid Prototyp. J.* 6 (2000) 155–161, <http://dx.doi.org/10.1108/13552540010337029>.
- [7] H.C.H. Ho, W.L. Cheung, I. Gibson, Effects of graphite powder on the laser sintering behaviour of polycarbonate, *Rapid Prototyp. J.* 8 (2002) 233–242, <http://dx.doi.org/10.1108/13552540210441148>.
- [8] K. Shahzad, J. Deckers, Z. Zhang, J.-P. Kruth, J. Vleugels, Additive manufacturing of zirconia parts by indirect selective laser sintering, *J. Eur. Ceram. Soc.* 34 (2014) 87–95, <http://dx.doi.org/10.1016/j.jeurceramsoc.2013.07.023>.
- [9] L. Cardon, J. Deckers, A. Verberckmoes, K. Ragaert, L. Delva, K. Shahzad, J. Vleugels, J.-P. Kruth, Polystyrene-coated alumina powder via dispersion polymerization for indirect selective laser sintering applications, *J. Appl. Polym. Sci.* 128 (2013) 2121–2128, <http://dx.doi.org/10.1002/app.38388>.
- [10] J. Deckers, J.-P. Kruth, K. Shahzad, J. Vleugels, Density improvement of alumina parts produced through selective laser sintering of alumina-polyamide composite powder, *CIRP Ann. – Manuf. Technol.* 61 (2012) 211–214, <http://dx.doi.org/10.1016/j.cirp.2012.03.032>.
- [11] K. Shahzad, J. Deckers, S. Boury, B. Neirinck, J.-P. Kruth, J. Vleugels, Preparation and indirect selective laser sintering of alumina/PA microspheres, *Ceram. Int.* 38 (2012) 1241–1247, <http://dx.doi.org/10.1016/j.ceramint.2011.08.055>.
- [12] E. Juste, F. Petit, V. Lardot, F. Cambier, Shaping of ceramic parts by selective laser melting of powder bed, *J. Mater. Res.* 29 (2014) 2086–2094, <http://dx.doi.org/10.1557/jmr.2014.127>.
- [13] J.P. Deckers, K. Shahzad, L. Cardon, M. Rombouts, J. Vleugels, J.-P. Kruth, Shaping ceramics through indirect selective laser sintering, *Rapid Prototyp. J.* 22 (2016) 544–558, <http://dx.doi.org/10.1108/RPJ-10-2014-0143>.
- [14] N. Mahato, A. Banerjee, A. Gupta, S. Omar, K. Balani, Progress in material selection for solid oxide fuel cell technology: a review, *Prog. Mater. Sci.* 72 (2015) 141–337, <http://dx.doi.org/10.1016/j.pmatsci.2015.01.001>.
- [15] X.Q. Cao, R. Vassen, D. Stoeber, Ceramic materials for thermal barrier coatings, *J. Eur. Ceram. Soc.* 24 (2004) 1–10, [http://dx.doi.org/10.1016/S0955-2219\(03\)00129-8](http://dx.doi.org/10.1016/S0955-2219(03)00129-8).
- [16] C. Piconi, G. Maccauro, Zirconia as a ceramic biomaterial, *Biomaterials* 20 (1999) 1–25, [http://dx.doi.org/10.1016/S0142-9612\(98\)00010-6](http://dx.doi.org/10.1016/S0142-9612(98)00010-6).
- [17] P. Bertrand, F. Bayle, C. Combe, P. Goeuriot, I. Smurov, Ceramic components manufacturing by selective laser sintering, *Appl. Surf. Sci.* 254 (2007) 989–992, <http://dx.doi.org/10.1016/j.apsusc.2007.08.085>.
- [18] Q. Liu, Y. Danlos, B. Song, B. Zhang, S. Yin, H. Liao, Effect of high-temperature preheating on the selective laser melting of yttria-stabilized zirconia ceramic, *J. Mater. Process. Technol.* 222 (2015) 61–74, <http://dx.doi.org/10.1016/j.jmatprotec.2015.02.036>.
- [19] ASTM B527-15, Standard Test Method for Tap Density of Metal Powders and Compounds, (2015).
- [20] I. Shishkovsky, I. Yadroitsev, P. Bertrand, I. Smurov, Alumina-zirconium ceramics synthesis by selective laser sintering/melting, *Appl. Surf. Sci.* 254 (2007) 966–970, <http://dx.doi.org/10.1016/j.apsusc.2007.09.001>.
- [21] Jan Wilkes, Yves-Christian Hagedorn, Wilhelm Meiners, Konrad Wissenbach, Additive manufacturing of ZrO<sub>2</sub>-Al<sub>2</sub>O<sub>3</sub> ceramic components by selective laser melting, *Rapid Prototyp. J.* 19 (2013) 51–57, <http://dx.doi.org/10.1108/13552541311292736>.
- [22] R.P. Ingel, D.L. Iii, Lattice parameters and density for Y<sub>2</sub>O<sub>3</sub>-stabilized ZrO<sub>2</sub>, *J. Am. Ceram. Soc.* 69 (1986) 325–332, <http://dx.doi.org/10.1111/j.1151-2916.1986.tb04741.x>.
- [23] A.L. Patterson, The scherrer formula for X-Ray particle size determination, *Phys. Rev.* 56 (1939) 978–982, <http://dx.doi.org/10.1103/PhysRev.56.978>.
- [24] F.W. Jones, The measurement of particle size by the X-ray method, *Proc. R. Soc. Lond. Math. Phys. Eng. Sci.* 166 (1938) 16–43.
- [25] A.N. Samant, N.B. Dahotre, Laser machining of structural ceramics – a review, *J. Eur. Ceram. Soc.* 29 (2009) 969–993, <http://dx.doi.org/10.1016/j.jeurceramsoc.2008.11.010>.
- [26] D. Triantafyllidis, L. Li, F.H. Stott, Crack-free densification of ceramics by laser surface treatment, *Surf. Coat. Technol.* 201 (2006) 3163–3173, <http://dx.doi.org/10.1016/j.surfcoat.2006.06.032>.
- [27] M. Mariño, M. Rieu, J.-P. Viricelle, F. Garrelie, Laser induced densification of cerium gadolinium oxide: application to single-chamber solid oxide fuel cells, *Appl. Surf. Sci.* 374 (2016) 370–374, <http://dx.doi.org/10.1016/j.apsusc.2015.12.220>.
- [28] P. Besnard, P.-N. Favennec, *Le laser et ses applications: 50 ans après son invention*, Hermès science publications, 2010.
- [29] Nikolay K. Tolochko, Maxim K. Arshinov, Andrey V. Gusarov, Victor I. Titov, Tahar Laoui, Ludo Froyen, Mechanisms of selective laser sintering and heat transfer in Ti powder, *Rapid Prototyp. J.* 9 (2003) 314–326, <http://dx.doi.org/10.1108/13552540310502211>.
- [30] J.-P. Kruth, P. Mercelis, J. Van Vaerenbergh, L. Froyen, M. Rombouts, Binding mechanisms in selective laser sintering and selective laser melting, *Rapid Prototyp. J.* 11 (2005) 26–36, <http://dx.doi.org/10.1108/13552540510573365>.